MnFe2O4 nanoparticles/cellulose acetate composite nanofiber for controllable release of naproxen

by Mochamad Zakki Fahmi

Submission date: 01-Sep-2021 08:52PM (UTC+0800)
Submission ID: 1639430414
File name: e2O4_nanoparticles-cellulose_acetate_composite_nanofiber_for.pdf (1.4M)
Word count: 6670
Character count: 35406

Materials Chemistry and Physics 250 (2020) 123055

Contents lists available at ScienceDirect

Materials Chemistry and Physics

journal homepage: www.elsevier.com/locate/matchemphys

$MnFe_2O_4$ nanoparticles/cellulose acetate composite nanofiber for controllable release of naproxen

Mochamad Zakki Fahmi [a,b,*], Roch Adi Prasetya [a], Muhammad Fathan Dzikri [a], Satya Candra Wibawa Sakti [a,b], Brian Yuliarto [c], Irzaman [d], Ferdiansjah [e]

[a] Department of Chemistry, Faculty of Science and Technology, Universitas Airlangga, Surabaya, 60115, Indonesia
[b] Supramodification Nano-Micro Engineering Research Group, Universitas Airlangga, Surabaya, 60115, Indonesia
[c] Department of Engineering Physics, Faculty of Industrial Technology, Institut Teknologi Bandung, Bandung, 40116, Indonesia
[d] Department of Physics, Bogor Agricultural University, Bogor, 16680, Indonesia
[e] Department of Nuclear and Technical Physics, Gadjah Mada University, Yogyakarta, 55281, Indonesia

HIGHLIGHTS

- Designing composite nanofiber from cellulose acetate, collagen, $MnFe_2O_4$ MNPs along with naproxen as drug loaded.
- Higher amount on MNPs give positive impact on make smaller nanofiber.
- Explore kinetical release of naproxen from nanofiber that accelerated by magnetic induction.
- The release mechanism of naproxen close to Korsmeyer-Peppas kinetics models with Fickian diffusion.

GRAPHICAL ABSTRACT

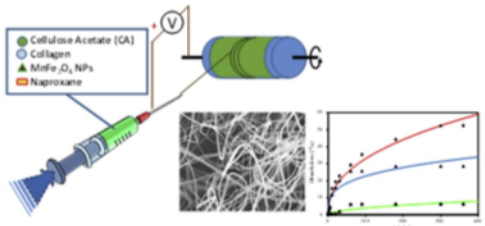

ARTICLE INFO

Keywords:
$MnFe_2O_4$ nanoparticles
Cellulose acetate
Naproxen
Nanofiber
Kinetic release

ABSTRACT

Nanofibers have been demonstrated to be highly effective for drug delivery applications. Although magnetic nanoparticles (MNPs) have been potentially added to nanofibers for improved drug release stimulation, the effect has been limited. In this study, a magnetic nanofiber membrane composed of cellulose acetate (CA), collagen (COL), and $MnFe_2O_4$ MNPs was prepared by electrospinning. Naproxen (NAP) drug was deposited on the nanofibers, and the drug release mechanism and effect of the MNPs on the stimulated NAP release were investigated. The electrical conductivity of the dope solution strongly affected the nanofiber characteristics. Moreover, the MTT cytotoxicity assay proved that CA-COL, CA-COL-NAP, and CA-COL-NAP-MNP nanofibers had low toxicity, as the cell viability was >80%. The NAP release mechanism was determined using zero-order, first-order, Higuchi, and Korsmeyer-Peppas kinetics models. According to the dissolution results, for all nanofibers, the NAP release followed the Korsmeyer-Peppas kinetics model, and the transport mechanism was Fickian diffusion. A high MNP concentration and neutral pH condition were conducive to NAP release.

* Corresponding author.
E-mail address: m.zakki.fahmi@fst.unair.ac.id (M.Z. Fahmi).

https://doi.org/10.1016/j.matchemphys.2020.123055
Received 3 January 2020; Received in revised form 7 April 2020; Accepted 9 April 2020
Available online 15 April 2020

1. Introduction

Electrospinning has received considerable attention in recent years because of its versatility and potential for applications in diverse fields [1,2]. Various polymers including natural and synthetic and hybrid materials have been successfully electrospun into nanofibers [3]. Nanofibers have been extensively studied because of their application potential in filtration [4], textiles [5], and biology, particularly for tissue engineering scaffolds and drug delivery devices [3]. One of the most promising applications is drug delivery [6]. Polymeric drug delivery systems have numerous advantages compared to conventional dosage forms. The release of pharmaceutical dosage using these systems can be designed as rapid, immediate, delayed, or modified dissolution and electrospun nanofiber scaffolds have been proven to be ideal matrices for wound healing owing to their unique properties such as high surface area to volume ratios and high porosity [7].

Clinically, one of the most effective ingredients used for wound healing and skin regeneration is collagen (COL), which is the main protein of the extracellular matrix (ECM). COL has been used for various applications in drug delivery and tissue engineering [8]. COL nanofibers are major components of the native ECM and related bio-derived polymer-based porous scaffolds [1,7]. However, electrospun COL scaffolds have low mechanical strength, especially in the hydrated state [2]. Thus, various attempts have been made to reinforce and improve the mechanical properties of COL materials; for example, COL has been blended with both synthetic and natural materials to obtain COL-based polymer blends or composites [4].

Polymers such as cellulose acetate (CA) and polycaprolactone (PCL) have been used for wound healing [6–8]. CA is a biopolymer commonly used for medicinal purposes because of its high hydrophilicity, good fluid transport properties, and water absorption capability [5]. Moreover, CA (acetate ester of cellulose) has been extensively electrospun into nanofibers with favorable properties such as good biocompatibility, biodegradation, regenerative properties, high affinity toward other substances, and tensile strength [9]. In addition, CA has excellent biocompatibility with the human body environment [10,11]. In contrast to PCL, CA is hydrophilic. The study of hydrophobic and hydrophilic properties of biomaterials is essential to determine their wettability for biomedical applications, such as wound healing, particularly because biomaterials will be in contact with blood, water, and other body fluids during their use [12]. Nanofiber membranes with good hydrophilicity and high porosity facilitate wound healing, particularly in the early healing phase [13]. For instance, it has been reported that hydrophilicity and bioactivity of CA promote cell proliferation and enhance the cellular interaction between scaffolds and fibroblast and improve the properties of nanofiber composites [11,14].

Recently, improvement design of wound healing nanofiber is focused on how to reach effective and efficient works of the fiber, including on covering an injury and delivering of a particular drug. Role of releasing drug and its way were crucial factors, where uncontrolled drug effect on high local concentration heading to increasing toxicity and emerging drug resistance [15]. Modification of the nanofiber structure and addition of outer components, such as nanoparticles, have been reported to be suitable methods to achieve sustained drug release [16,17]. Magnetic nanoparticles (MNPs) are extensively used because of their unique multifunctional properties. However, reports on the application of magnetic nanofibers for drug delivery are rare. Sasikala et al. incorporated iron oxide MNPs into polymer nanofibers, and they found that the MNPs triggered the release of drug in hyperthermia treatment [18]. Moreover, this finding remains the challenges, especially, how the role of drug releasing from a nanofiber and its kinetic that is not clearly explored yet.

Among several kind of MNPs, $MnFe_2O_4$ MNPs have known performing several advantages, such as low toxicity, superparamagnetic property, easy on producibility, and biocompatibility [19–21]. All the above advantages and its unique response on magnetic field made $MnFe_2O_4$ MNPs become multiple functionalities of triggered drug release. In the present study, we develop a composite nanofiber that can overcome emerged problems from previous report. The novel of this report is addressed to a blended CA-COL with $MnFe_2O_4$ MNPs to obtain magnetic hybrid nanofibers that never reported before. Moreover, a new drug delivery system was developed using this magnetic induced nanofiber by naproxen (NAP; a non-steroidal anti-inflammatory drug) loading. Initiated by investigating the effects of MNPs on morphology and structure of the fiber, this study further evaluates toxicity effect along with observation on kinetically release of NAP upon magnetic hybrid nanofiber. The composite nanofibers were found to be well formed, nontoxic, and magnetic influenced on NAP release. The release pattern of NAP mostly followed the Korsmeyer-Peppas kinetic model and neutral conditions facilitated the release.

2. Materials and methods

2.1. Materials

Cellulose acetate (Mw) 30.000 g.mol-1 (CA), sodium hydroxide (98.5%, NaOH), chloroform (99%), benzyl ether (98%), acetone (99.5%), oleylamine (70%), mangan (II) acetylacetonate (100%, Mn $(acac)_2$) and iron (III) acetylacetonate (100%, $Fe(acac)_3$), sodium naproxene (98%) were purchased from Sigma-Aldrich, USA. Medium of buffer solutions (pH 4 and pH 9) and Phosphate buffered saline (100%, PBS) were purchased from Merck, Germany. Bovine collagen was purchased from commercial products of Gelita, Brazil. All of chemical were directly used without particular purification.

2.2. Synthesis of nanoparticle $MnFe_2O_4$

$MnFe_2O_4$ MNPs were prepared following the previous report.[32] Experimentally, about 2 mmol of $Fe(acac)_3$ and 1 mmol of $Mn(acac)_2$ are mixed in the solution of 15 mL oleylamine and 15 mL benzyl ether. The mixture solution was further stirred and heated up to 300 °C for 1 h under argon flow. After the temperature cooling down to room temperature, the resulted MNPs were pressed down by add ethanol and centrifugation (6000 rpm for 10 min).

2.3. Electrospinning preparation of CA-COL- NAP-MNPs magnetic nanofiber

On the first step, the electrospinning dope solution was prepared by blend CA solution in acetone (30 mg/mL) and COL in aqueous solution (20 mg/mL) under magnetic stirrer to form a homogeneous solution. The $MnFe_2O_4$ MNPs in chloroform were subsequently added to the blended polymer solution and mixed for 2 h following by naproxen solution in NaOH (20 mg/mL 0.1 N). The electrospinning processes is illustrated in Scheme 1, in which the solution was transferred to 10 mL syringe mounted onto a syringe pump with a 20G metallic needle. Electrospinning equipped with a flat/cylinder collector was operated in a high voltage power supply 12 kV. The flow rate of the polymer solution was varied to 0.1, 0.3, 0.5, and 0.7 μL h^{-1}. Meanwhile, the optimization of running time was done adjusted time on 1, 3, 5, and 7 h. The resulted fiber was collected on a ground collector covered by a flat/cylinder aluminum foil. The distance between the needle tip and the target was set at 12 cm. The resulted magnetic nanofiber, composing cellulose acetate-collagen-naproxen-$MnFe_2O_4$ nanoparticle is represented as CA-COL-NAP-MNPs. The concentration of MNPs on the magnetic nanofiber also varied on 1, 3, and 5 g that also represented as CA-COL-NAP-MNPs 1, CA-COL-NAP-MNPs 3, and CA-COL-NAP-MNPs 5, respectively.

2.4. Cytotoxicity analysis

The toxicity assessment of obtained nanofiber was analyzed via MTT assay (Sigma - Aldrich). Prior to this *in vitro* assay, HeLa cells were

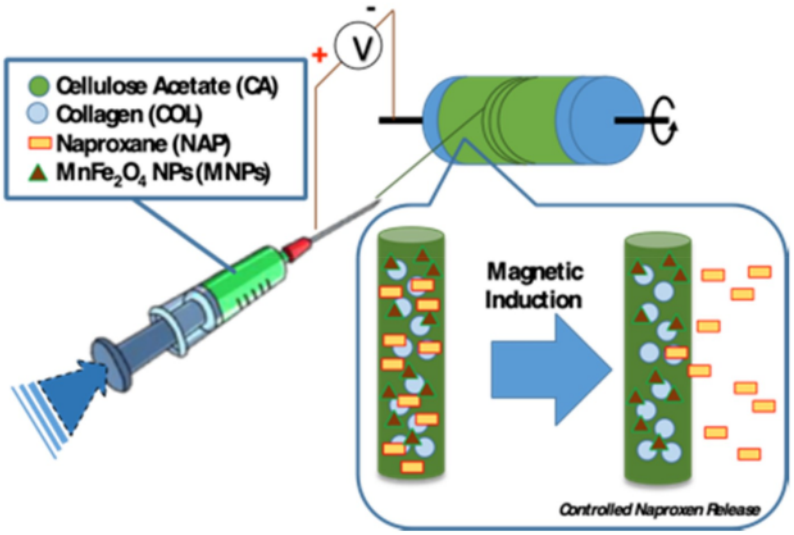

Scheme 1. Schematic illustration of preparing CA-COL-NAP-MNPs nanofiber. Naproxen was embedded into nanofiber and MNPs provide control release.

preserved on DMEM medium and stored at incubator with maintained condition on humidified 5% CO_2 and temperature at 37 °C. On HeLa culturing day, the nanofiber sample was put at each 24 well with 0.5 × 0.5 cm^2 in size and added with 200 μL medium along with HeLa cell was seed on each well with a density of 5.4 × 10^4 and let to grow for 24 h. The cell medium further removed; washed with PBS and added with 300 μl medium containing MTT (DMEM 270 μL + MTT 30 μL). The cell was incubated for other 4 h and the precipitate formed by the MTT result was dissolved by the addition of 200 mL of DMSO. Absorbance measured at 560 nm wavelengths using GloMax-Multi Microplate Multimode Reader (Promega, USA). The higher absorbance on the MTT results correlate with higher living cell and compared with controls, which is untreated HeLa. All MTT results were stated as toxic if its viability percentage of HeLa less than 80%.

2.5. NAP release and its kinetic evaluation

To verify kinetic release of NAP, the fiber mat sample (2 × 2 cm^2) was placed on dialysis membrane MWCO (40 kDa) and immersing the membrane on 50 mL of DI water on a beaker. This set was then placed on magnetic stirrer without magnetic bar and ran with magnetic round of 200 rpm. At regulated times, 1 mL of supernatant was taken from outer membrane and the total volume is kept on 50 mL by adding fresh DI Water. The amount of NAP released was measured using a UV–Vis spectrophotometer by measuring the absorbance at 330.5 nm and refers to calibration data of NAP standard solutions. The actual concentration of released naproxen was determined with follow below equation:[32]

$$C_{act} = C_{mea} + \frac{v}{V}\sum_{0}^{i-t} C_{mea} \quad (1)$$

where C_{act} (ppm) is the actual concentration at time t (s), C_{mea} the measured concentration at time t (ppm), v is the volume of the DI water taken (mL), and V is the total volume of the DI water (mL).

The mechanism of NAP release was fitted by study its dissolution profile with four kinetic models, namely the zero order, first order, Higuchi, and Korsmeyer-Peppas, which is performed as Equations (2)–(5), respectively.

$$F_t = K_0 \cdot t \quad (2)$$

where F_t refers to the fraction of released NAP in time t and K_o is the zero-order release constant (s^{-1}).

$$\ln\ (1 - F_t) = -K_1 \cdot t \quad (3)$$

where F_t refers to the fraction of released NAP in time t and K_1 is the first-order release constant (s^{-1}).

$$F_H = K_2 \cdot t^{1/2} \quad (4)$$

where F_H refers to the fraction of released NAP in time t and K_2 is Higuchi release constant ($s^{-0.5}$) [8].

$$\frac{M_t}{M_\infty} = K_3 \cdot t^n \quad (5)$$

where M_t and M_∞ refer to the amount of NAP released at time t and ∞, respectively, K_3 is Korsmeyer-Peppas release costant and n is release exponent. The value of n indicates Fickian diffusion If $n \leq 0.5$, non-Fickian or anomalous phenomena if $0.5 < n < 1$, and $n \geq 1$ imply to lack of time dependence on release kinetics; i.e., zero-order kinetics.

2.6. Characterizations

The morphology of nanofiber membrane was observed by using scanning electron microscope (SEM, Zeiss EVO MA-10). Fiber diameter was calculated from the SEM images by using an image J analysis software. The crystal structure of the nanoparticles was determined using X-ray diffraction (XRD, Rigaku D/Max-2BX) with Cu Kα radiation on 2θ range of 5°–65°. The particle size distributions of MNPs were determined in aqueous solutions with dynamic light scattering (DLS, Zetasizer nano ZS Malvern) equipped with a 633 nm He–Ne laser. For topology analysis, MNPs powder was observed by transmission electron microscope (TEM, Philips Tecnai G2 F20 microscope) attributed with energy dispersed X-ray spectroscopy (EDS) detector with an accelerating voltage of 200 kV. MNPs sample for TEM observations was prepared by dropping a dilute solution of the NPs onto 200 mesh copper grids coated with a thin Formvar–carbon film and allowing the solvent to evaporate in air at room temperature. The diameter size of obtained fiber was measured from SEM images and analyzed with Image J software, which it was limited on 50 fibers per SEM micrograph. Conductivity of nanofiber was measured from fiber solutions using Conductivity meter (JP

analysis was be done using thermal gravimetric analysis (TGA, PerkinElmer TGA 4000) from 40 to 995 °C with rate 10 °C/min.

3. Results

3.1. Synthesis and characterization of nanoparticle

$MnFe_2O_4$ MNPs were prepared by the solvothermal method with Mn $(acac)_2$ and $Fe(acac)_3$ as the precursors. The purity and crystallinity of the $MnFe_2O_4$ MNPs were characterized by powder XRD and the XRD pattern is shown in Fig. 1. The XRD pattern of the prepared MNPs shows distinct peaks at $2\theta = 18, 29.70, 34.98, 36.65, 42.53, 52.74, 56.19$, and $61.66°$.

The TEM image of $MnFe_2O_4$ MNPs (Fig. 2a) shows particles with diameters in the range of 2–20 nm. The high-magnification images (red squares in Fig. 2a) clearly reveal the actual size and near-spherical morphology of the particles. The corresponding EDX profile (Fig. 2b) reveals the presence of Mn, Fe, and O, indicating the formation of $MnFe_2O_4$ MNPs, in agreement with the XRD data. In addition, DLS was performed to comprehensively determine the diameter of the MNPs, and corrected TEM result on observing MNPs size. The DLS graph in Fig. 2c shows that the maximum particle size (highest peak) is 28.21 nm.

3.2. Electrospinning process

In the electrospinning process, a high voltage is applied between the spinnerets and the metal collector, converting the half-spherical surface of the polymer solution into a cone, called the Taylor cone [22]. In the present study, we optimized the formation of the Taylor cone by tuning the flow rate of the dope solution. As shown in Fig. S1 (Supporting Information), the Taylor cone formed at a flow rate of 0.01 μl h^{-1} rapidly dries before the fibers reach the collector. A more stable Taylor cone is formed at a higher flow rate of 0.05 μl h^{-1}. However, with further increase in the flow rate (0.1, 0.15, and 0.2 μl h^{-1}), the Taylor cone becomes unstable. Therefore, the optimum flow rate for nanofiber formation was determined to be 0.05 μl h^{-1}. Further optimization was performed by varying the process time from 1 h to 7 h (see Fig. S2, Supporting Information).

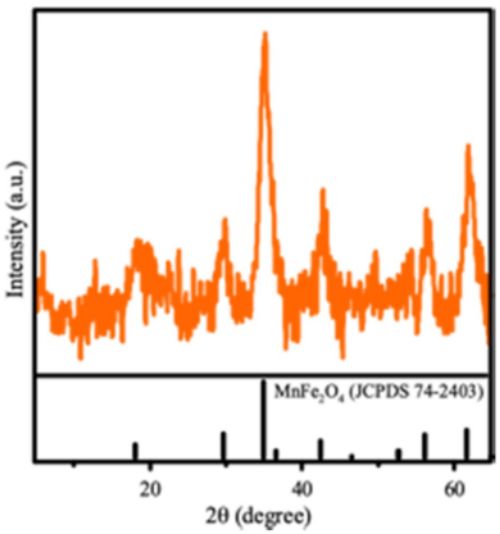

Fig. 1. XRD pattern of $MnFe_2O_4$ nanoparticle.

3.3. Characterization of the nanofiber membrane

The magnetic nanofiber membrane prepared by electrospinning was characterized by SEM, SEM-EDX, Fourier-transform infrared (FTIR) spectroscopy, and TGA. Morphological observation of the magnetic membrane was carried out with an SEM instrument (Fig. 3). The SEM images indicate the successful formation of nanosized composite fibers. Moreover, with the addition of COL and NAP to the electrospinning solution, nanofibers with diameters lower than those of CA nanofibers are formed. As shown in Table 1, the diameters of nanofibers composed of CA, COL, NAP, and MNPs are lower than those of CA nanofibers. Conductivity measurements performed on the dope solution (Table 1) show that the conductivity of CA solution is approximately 0.8 μS cm^{-1}, and after the addition of COL and NAP, the conductivity increases to 3.5 μS cm^{-1}. Moreover, the conductivity of the dope solution containing MNPs varies with the concentration of MNPs; the conductivities of CA-COL-NAP-MNPs 1, 3, and 5 solutions are 14.7, 17.8, and 22.5 μS cm^{-1} respectively. These results indicate that with increasing dope solution conductivity, the nanofiber diameter decreases.

SEM-EDX images (showed on supporting information, Fig. S3) showed any elements constructing the nanofiber, where it shows Na, Fe, and Mn peaks elements. To validate the EDX data, FTIR analysis was carried out and the FTIR spectrum of the magnetic nanofibers was compared with those of the components of the nanofibers (Fig. 4a). The FTIR spectra of pure CA, NAP, and COL, and magnetic nanofibers show similar absorption bands at around 1760 cm^{-1} assigned to C=O stretching and 902 cm^{-1} assigned to the acetyl group of C–O stretching. In addition, the FTIR spectra of NAP and COL are quite similar, with bands at 1726 cm^{-1} (C=O), 2962 cm^{-1} (CH_3), 3003 cm^{-1} (O–CH_3), and 3145 cm^{-1} (OH-). MNPs exhibit sharp bands at 2963, 2843, and 806 cm^{-1} corresponding to C–H symmetric stretching, asymmetric stretching, and bending vibrations, respectively; in addition, the MNPs exhibit a band at 1266 cm^{-1} corresponding to aliphatic C–C, and crowded bands at around 500 cm^{-1} corresponding to spinel ferrite bonds [23]. The TGA plots (Fig. 4b) show weight reduction at 200–400 °C for the MNP sample, and significant mass losses at 392, 278, and 221 °C, for CA, NAP, and COL samples, respectively.

3.4. Cytotoxicity evaluation

The cytotoxicity evaluation was carried out by immersing the adjusted shape of nanofiber and measure HeLa tumor cell viability against time via MTT assay. HeLa cells were treated with CA-COL, CA-COL-NAP, and CA-COL-NAP-MNPs for 0.5, 1, 1.5, 2, 2.5, and 3 days. The results presented in Fig. 5 reveal that the percentage of cell viability in the presence of CA-COL nanofibers is >80% for up to three days. In addition, the percentage viability of HeLa cells incubated with CA-COL-NAP nanofibers is >80%. In the presence of the CA-COL-NAP-MNP sample, the cell viability is >80% for up to three days.

3.5. In vitro NAP release and its kinetic evaluation

The mechanism of drug release from the polymer composites was determined by dissolution tests; the results were fitted with four kinetic models: zero-order, first-order, Higuchi, Korsmeyer-Peppas models. The release rate of NAP under magnetic induction (using a rotary magnetic stirrer) was determined. From the data in Fig. 6, it can be seen that from all NAP-loaded nanofibers, in the initial stage (first 30 min), burst release occurs, followed by sustained release. In addition, the figure shows the comparison between the experimental and kinetic model results. It can be observed that that the Korsmeyer-Peppas model best fits the experimental data. As can be observed from Table 2, R^2 value is the highest for the Korsmeyer-Peppas model. Moreover, the addition of MNPs accelerates the release of NAP.

Moreover, the effect of pH on NAP release was investigated. As observed from Fig. 7 and Table 3, at all pH values, the release follows the

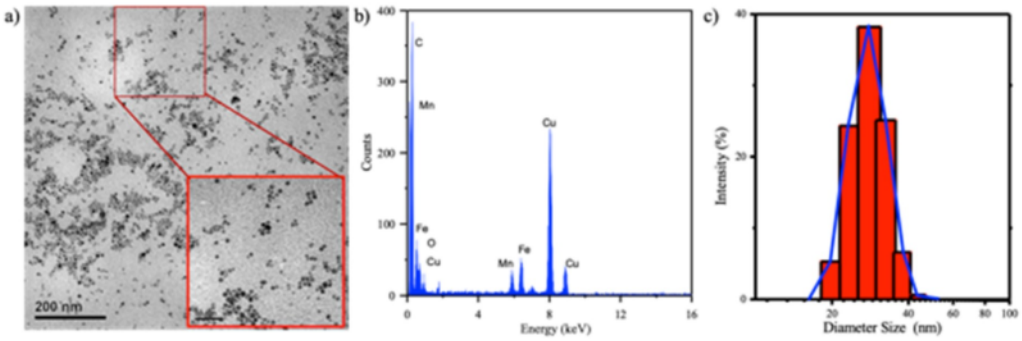

Fig. 2. TEM images of MNPS (a) and its EDX result (b). Red box of TEM images showed higher magnification images on the determined area. (c) DLS results of MNPs nanoparticle. (For interpretation of the references to colour in this figure legend, the reader is referred to the Web version of this article.)

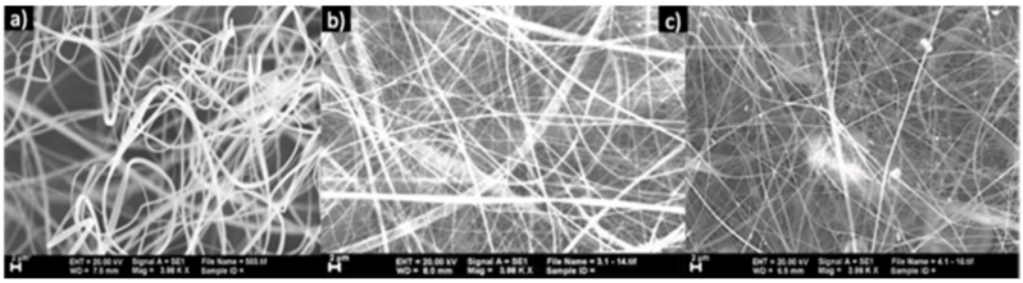

Fig. 3. SEM Images of (a) CA, (b) CA-COL-NAP, and (c) CA-COL-NAP-MNPs nanofiber.

Table 1
Average diameter size of nanofiber (n = 50).

Nanofiber Sample	Diameter (nm)[a]	Conductivity (μS.cm^{-1})
CA	475 ± 25	0.8
CA-COL-NAP	407 ± 35	3.5
CA-COL-NAP-MNPs 1	293 ± 42	14.7
CA-COL-NAP-MNPs 3	302 ± 62	17.8
CA-COL-NAP-MNPs 5	279 ± 28	22.5

[a] All data were presented as mean ± SD (n = 50).

Korsmeyer-Peppas kinetics model and Fickian diffusion (n < 0.5). Notably, the dissolution rate (variation in dissolution percentage with time) at pH 7 is higher than those at pH 4 and 9.

4. Discussion

Modification of nanofibers via the addition of $MnFe_2O_4$ magnetic nanoparticles significantly enhances the application potential of nanofibers in medicine, particularly for drug delivery. The utilization of COL nanofibers reinforced with CA and modified with $MnFe_2O_4$ MNPs and NAP can considerably improve the drug release mechanism. However, before any application, it is imperative to investigate the properties of the MNPs, nanofibers, and magnetic nanofibers.

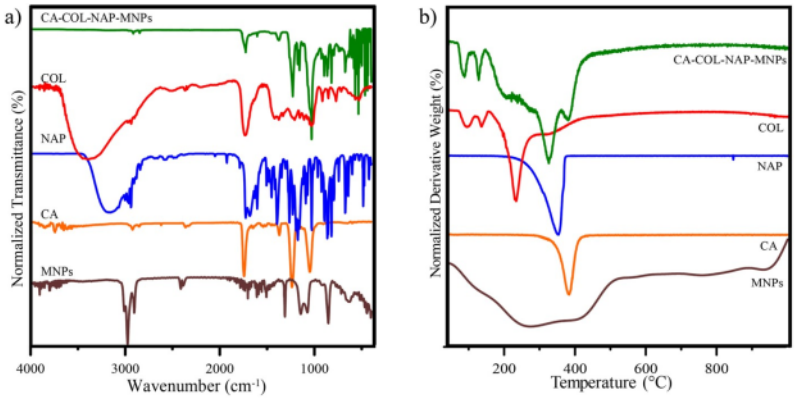

Fig. 4. (a) FTIR spectra and (b) TGA curves as derivate % weights, data of the magnetic nanofiber comparing with its components.

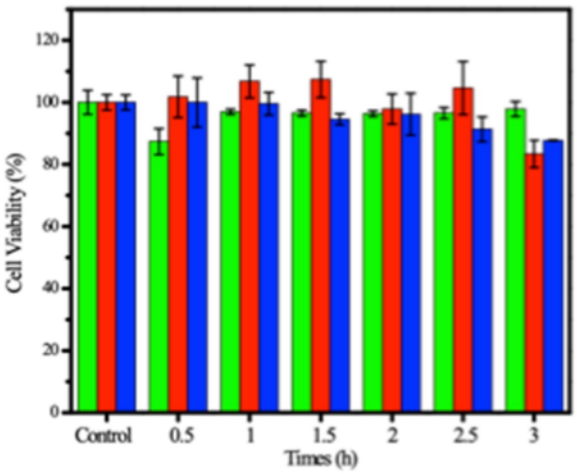

Fig. 5. Cell viability data of HeLa cell after adjusted times incubation with CA-COL (green); CA-COL-NAP(red); and CA-COL-NAP-MNPs (blue). All data is represented as means ± SD (n = 3). (For interpretation of the references to colour in this figure legend, the reader is referred to the Web version of this article.)

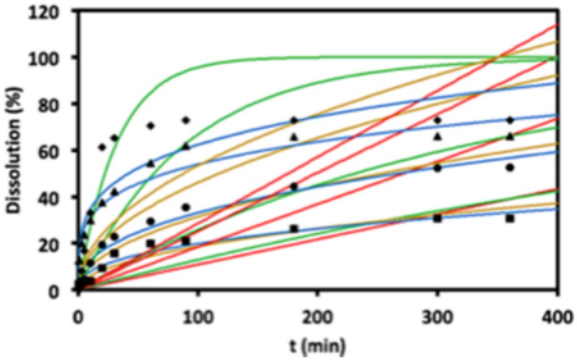

Fig. 6. Dissolution rate of NAP from CA-COL-NAP (■), CA-COL-NAP-MNPs 1 (●), CA-COL-NAP-MNPs 2(▲) and CA-COL-NAP-MNPs 3(◆) nanofibers. Fitted curves following kinetic models of each sample are represented on red line (zero order); green line (first order); brown line (Higuchi); and blue line (Koresmeyer-peppas). (For interpretation of the references to colour in this figure legend, the reader is referred to the Web version of this article.)

Crystal structure, morphological, and elemental analyses were carried out to prove the formation of $MnFe_2O_4$ MNPs. The XRD pattern of the MNP sample matches with that of the standard $MnFe_2O_4$ sample (JCPDS No. 10-0319), confirming the successful formation of $MnFe_2O_4$ nanoparticles.

The TEM images reveal that the MNPs are spherical in shape. In addition, the TEM images show that each MNP is covered by oleylamine, resulting in the formation of interparticle spaces. Thus, the addition of oleylamine as a capping agent stabilizes the MNPs, preventing the accumulation of iron and manganese oxide in the MNPs. All the presented data confirm the successful synthesis of $MnFe_2O_4$ MNPs.

Magnetic nanofibers were prepared by electrospinning at a high voltage. The solution of nanofiber composition was blended with various concentration of $MnFe_2O_4$ MNPs. With increasing flow rate of the dope solution up to 0.05 μl h^{-1}, the stability of the Taylor cone increases. The dope solution attracted and attached on the surface of the collector due to applied a high voltage. The higher flow rate causes the balance between the rate of released dope solutions to the target and volatile rate of solvent on the dope solution. Moreover, the flow rate affects the nanofiber diameter; a minimum flow rate is preferred to maintain a balance on the released dope solution and the replacement of the solution during jet formation [10]. The nanofibers formed in a short operating time cannot be peeled from the aluminum foil because of its thin layer; notably, changing the electrospinning process time does not significantly affect the diameter and structure of the formed nanofibers [14].

The formed magnetic nanofibers possess the beneficial characteristics of each component. Whilst NAP drug embedded on the nanofiber, CA is in charge on strengthening nanofiber from physical inferences. Moreover, COL was added to enhance the biocompatibility of the nanofibers and MNPs were added to control the release of NAP under magnetic induction. The variation in the nanofiber diameter after COL, NAP, and MNP addition (Table 1) is mainly attributed to the changes in viscosity and electrical conductivity of the dope solution. The addition of NAP and COL dissolved in a polar solvent leads to a decrease in the viscosity of the dope solution with acetone as the main solvent [24]. After the incorporation of MNPs, the conductivity increases because MNPs contain metal ions, which increase the electropositive charge of the dope. Thus, the dope is accelerated toward the collector. The SEM results further confirm the conductivity data for the dope solution

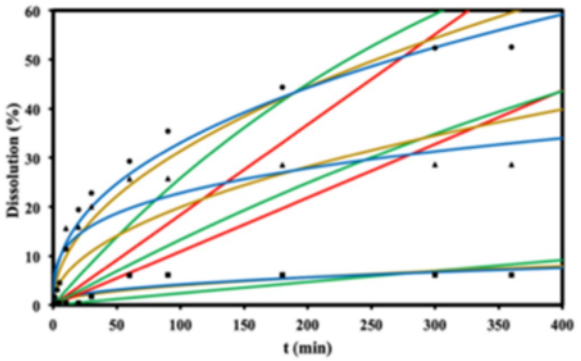

Fig. 7. Dissolution rate of NAP from CA-COL-NAP-MNPs 1 on pH 4 (■), pH 7 (●), and pH 9(▲). Fitted curves following kinetic models of each sample are represented on red line (zero order); green line (first order); brown line (Higuchi); and blue line (Korsmeyer-Peppas). (For interpretation of the references to colour in this figure legend, the reader is referred to the Web version of this article.)

Table 2
NAP kinetic release of nanofiber on varied MNPs amount.

Nanofiber Sample	Zero Order		First Order		Higuchi		Korsmeyer Peppas		
	K_0	R^2	K_1	R^2	K_2	R^2	K_3	R^2	n
CA-COL-NAP	0.00108	0.79595	0.00138	0.83312	1.85789	0.93850	3.09412	0.95615	0.40311
CA-COL-NAP-MNPs 1	0.00184	0.81100	0.00299	0.88414	3.13812	0.95662	4.77776	0.97411	0.42006
CA-COL-NAP-MNPs 3	0.00251	0.63329	0.01100	0.90806	4.60735	0.84419	17.87851	0.94658	0.23938
CA-COL-NAP-MNPs 5	0.00285	0.41117	0.03113	0.91303	5.33021	0.63612	19.23987	0.78298	0.25512

Table 3
NAP kinetic release of nanofiber on varied pH.

CA-COL-NAP-MNPs Sample	Zero Order		First Order		Higuchi		Korsmeyer Peppas		
	K_0	R^2	K_1	R^2	K_2	R^2	K_3	R^2	n
pH 4	0.00023	0.60591	0.00024	0.61396	0.39826	0.77401	0.58474	0.79277	0.42725
pH 7	0.00184	0.81100	0.00299	0.88414	3.13812	0.95662	4.77776	0.97411	0.42006
pH 9	0.00109	0.53718	0.00143	0.58152	1.99286	0.75695	6.05252	0.86552	0.28804

(Table 1) and the data are in good agreement with those previously reported; it has been demonstrated that with increasing electrical conductivity of the spinning solution, the fiber diameter decreases and with increasing viscosity of the solution, the fiber diameter increases [25]. However, the effect of electrical conductivity is more dominant than that of the viscosity of the solution. An increase in the electrical conductivity increases the electrical charge of the polymer jet during the electrospinning process [26]. As a result, the level of draw and large draw ratio of the jet in the flexural instability area can increase during electrospinning. The unstable polymer jet causes elongation and stretching of the fibers, thereby reducing the fiber diameter [27].

The SEM-EDX results confirm that the chemical composition of the magnetic nanofibers is as expected. Qualitatively, the sodium peak from NAP sodium confirms the presence of NAP. Moreover, the Fe and Mn peaks confirm the presence of $MnFe_2O_4$ MNPs in the nanofiber membrane. The calculation of elements percentage also proves it by comparison of the percentage of O to C atoms in Fig. S3b is greater than in Fig. S3a due to contribution of O atom from MNPs. The FTIR spectrum of the magnetic nanofiber sample show absorption bands assigned to C=O stretching (1760 cm^{-1}) and the acetyl group of C–O stretching (902 cm^{-1}), proving the existence of CA, NAP, and COL. The NAP and COL possess similar spectrum for several functional groups, however the broader band and right shifting on COL are most caused by complicated hydrogen binding on hydroxyl moieties of proteins. The magnetic nanofiber sample shows sharp bands at 2963, 2843, 806, 1255, and 500 cm^{-1} due to oleylamine, which was used a as capping agent for MNPs, and absorption bands corresponding to spinel ferrite. Analyses of FTIR spectra indicates there is no new peaks appeared and each spectrum also exist on CA-COL-NAP-MNPs spectra. It means that attraction of any components of nanofiber close to physical bonding, such as hydrogen bounding, van der Waals, and π-π attractions. This phenomenon is further supported by the TGA results (Fig. 4b); the derivative curve of decreasing weight of CA-COL-NAP-MNPs is composed precisely of its components referring no chemical bonding formatted on the magnetic nanofiber. The weight reduction for MNPs in the range of 200–400 °C is mostly attributed to evaporation and removal of oleylamine on the surface of MNPs. Significant mass losses for CA at 392 °C, NAP at 278 °C, and COL at 221 °C indicate their extensive degradation, and the dehydration of COL at the initial temperature.

Because the nanofibers were prepared for NAP delivery in wound healing, the investigation of toxicity of the nanofibers was an important part of this study. The MTT assay results for CA-COL nanofibers indicate low toxicity, as the percentage of cell viability is higher than 80%. The MTT assay result agrees with the earlier finding that CA and COL have good biocompatibility, which makes them suitable for biomedical applications, as mentioned in the introduction of this report. Moreover, the addition of NAP and COL significantly decreases the HeLa cell percentage viability. Even up to three days, the percentage viability of HeLa cells incubated with CA-COL-NAP and CA-COL-NAP-MNPs is more than 80%. The cells freely stack and proliferate on the nanofibers, as shown in Fig. S4, Supporting Information. This clearly proves that the toxicity effect of the nanofibers is low.

To determine the drug release mechanism, the dissolution test results for the magnetic nanofibers were analyzed using kinetic models. The NAP release (Fig. 6) closely follows the Korsmeyer-Peppas model; the R^2 value is the highest for this model (Table 2). Moreover, with increasing MNP concentration on the nanofibers, the kinetic constant for NAP release increases. Once the rotary magnetic induction is given, MNPs will response and deliver it as the dynamic of nanofiber enable a boost for NAP as small molecule to left nanofiber.

Unlike the Higuchi model, which describes the release of drug from the general drug matrix, the Korsmeyer-Peppas model is designed for drug release specifically from a polymeric system, where the drug must overcome the polymer hurdle during the release process [28]. This indicates that CA and COL influence the NAP release, and even, accelerate it in the presence of MNPs. Furthermore, the n value for the Korsmeyer-Peppas model for all nanofibers is < 0.5, indicating that NAP release follows Fickian diffusion; this confirms that NAP release is based on the formation of concentration gradients. While the concentration of MNPs on the membrane is high, like CA-COL-NAP-MNPs 5, the NAP release tends to follow the first-order kinetics model (based on the R^2 value, Table 2), which match to releasing model of drug that disturbed with adsorption or elimination of drug from porous matrices [29]. This indicates that MNPs have the potential to adsorb NAP.

Furthermore, the release of NAP at all pH values follows the Korsmeyer-Peppas model and Fickian diffusion (Fig. 7 and Table 3). The percentage of dissolution at pH 4 and 9 is low, possibly because of the enhanced electrostatic attraction of the nanofibers. NAP dissolves well in a slightly basic medium; notably, the nanofiber contains abundant moieties on high potency to perform electronegative charge, like carboxylate and hydroxyl groups. This will lead to high electrostatic repulsion. Therefore, under a basic condition, NAP that possesses electronegative moieties will be repelled by the nanofibers. However, comparing with neutral condition (pH 7), the fiber on high electronegative charge perform higher molecular dynamic on the system, where it affect not only to drive away NAP, but also draw it back to the fiber. The emerging electronegative part also will be stabilized by approaching electropositive part on this system and forming a stronger attraction, in which affected the diffusion of the NAP. Thus, the NAP release rate under a base basic condition is lower than that under a neutral condition. At a final, these finding prove potential application of MNPs composited nanofiber on encourage release of drug loaded on. Even has been explored data and proved the potential contribution of MNP to drug release, the current report acts as preliminary study on design wound healing nanofiber membrane that can accelerate release of its drug by magnetic induction.

5. Conclusions

In this study, composite nanofibers containing CA, COL, NAP, and $MnFe_2O_4$ MNPs were successfully synthesized by electrospinning. The MNPs magnetic nanoparticles were well characterized and, with NAP, incorporated on the nanofiber to form magnetic nanofiber, which further effect on reduced the diameter size of nanofiber. All nanofibers exhibited low toxicity toward HeLa cells for three days. Moreover, the MNPs facilitated the release of NAP, and the release of NAP could be controlled by adjusting the concentration of MNPs, thereby avoiding the need to control the intensity of magnetic induction. Notably, the NAP release rate was higher in the neutral pH condition than in the basic or acidic condition, because of minimum electrostatic attraction in neutral pH. The release of NAP from the nanofibers follows the Korsmeyer-Peppas kinetic model, according to which, the drug release mechanism is influenced by CA and COL.

Declaration of competing interest

The authors declare that they have no known competing financial interests or personal relationships that could have appeared to influence the work reported in this paper.

CRediT authorship contribution statement

Mochamad Zakki Fahmi: Conceptualization, Writing - review & editing, Supervision. **Roch Adi Prasetya:** Project administration. **Muhammad Fathan Dzikri:** Investigation. **Satya Candra Wibawa Sakti:** Validation. **Brian Yuliarto:** Funding acquisition. **Irzaman:** Funding acquisition. **Ferdiansjah:** Funding acquisition.

Acknowledgements

Authors thank to Universitas Airlangga and Ministry of Research, Technology and Higher Education, Republic of Indonesia for financial support on RKI project under contract no. 563/UN3.14/LT/2019.

Appendix A. Supplementary data

Taylor cone images on varied flow rate; the nanofiber images on varied electrospinning collector; EDX data of nanofiber and HeLa cell images stacking on the nanofiber.

Supplementary data to this article can be found online at https://doi.org/10.1016/j.matchemphys.2020.123055.

References

[1] S. Agarwal, A. Greiner, J.H. Wendorff, Functional materials by electrospinning of polymers, Prog. Polym. Sci. 38 (2013) 963–991.
[2] N. Bhardwaj, S.C. Kundu, Electrospinning: a fascinating fiber fabrication technique, Biotechnol. Adv. 28 (2010) 325–347.
[3] Z.-M. Huang, Y.-Z. Zhang, M. Kotaki, S. Ramakrishna, A review on polymer nanofibers by electrospinning and their applications in nanocomposites, Compos. Sci. Technol. 63 (2003) 2223–2253.
[4] F. Dotti, A. Varesano, A. Montarsolo, A. Aluigi, C. Tonin, G. Mazzuchetti, Electrospun porous mats for high efficiency filtration, J. Ind. Textil. 37 (2007) 151–162.
[5] A. Zucchelli, M.L. Focarete, C. Gualandi, S. Ramakrishna, Electrospun nanofibers for enhancing structural performance of composite materials, Polym. Adv. Technol. 22 (2011) 339–349.
[6] T.J. Sill, H.A. von Recum, Electrospinning: applications in drug delivery and tissue engineering, Biomaterials 29 (2008) 1989–2006.
[7] S. Tungprapa, I. Jangchud, P. Supaphol, Release characteristics of four model drugs from drug-loaded electrospun cellulose acetate fiber mats, Polymer 48 (2007) 5030–5041.
[8] T.P. Armedya, M.F. Dzikri, S.C.W. Sakti, A. Abdulloh, Y. Raharjo, S. Wafiroh, M. Z. Fahmi, Kinetical release study of copper ferrite nanoparticle incorporated on PCL/collagen nanofiber for naproxen delivery, BioNanoScience 9 (2019) 274–284.
[9] R. Konwarh, N. Karak, M. Misra, Electrospun cellulose acetate nanofibers: the present status and gamut of biotechnological applications, Biotechnol. Adv. 31 (2013) 421–437.
[10] A.R. Unnithan, G. Gnanasekaran, Y. Sathishkumar, Y.S. Lee, C.S. Kim, Electrospun antibacterial polyurethane–cellulose acetate–zein composite mats for wound dressing, Carbohydr. Polym. 102 (2014) 884–892.
[11] S. Fischer, K. Thümmler, B. Volkert, K. Hettrich, I. Schmidt, K. Fischer, Properties and applications of cellulose acetate, in: Macromolecular Symposia, Wiley Online Library, 2008, pp. 89–96.
[12] R.A. Gittens, L. Scheideler, F. Rupp, S.L. Hyzy, J. Geis-Gerstorfer, Z. Schwartz, B. D. Boyan, A review on the wettability of dental implant surfaces II: biological and clinical aspects, Acta Biomater. 10 (2014) 2907–2918.
[13] J.A. Matthews, G.E. Wnek, D.G. Simpson, G.L. Bowlin, Electrospinning of collagen nanofibers, Biomacromolecules 3 (2002) 232–238.
[14] T. Heinze, T. Liebert, 4.2 Chemical characteristics of cellulose acetate, in: Macromolecular Symposia, Wiley Online Library, 2004, pp. 167–238.
[15] S.-F. Chou, D. Carson, K.A. Woodrow, Current strategies for sustaining drug release from electrospun nanofibers, J. Contr. Release 220 (2015) 584–591.
[16] H. Yu, P. Yang, Y. Jia, Y. Zhang, Q. Ye, S. Zeng, Regulation of biphasic drug release behavior by graphene oxide in polyvinyl pyrrolidone/poly (ε-caprolactone) core/sheath nanofiber mats, Colloids Surf. B Biointerfaces 146 (2016) 63–69.
[17] J.G. Merrell, S.W. McLaughlin, L. Tie, C.T. Laurencin, A.F. Chen, L.S. Nair, Curcumin-loaded poly (ε-caprolactone) nanofibres: diabetic wound dressing with anti-oxidant and anti-inflammatory properties, Clin. Exp. Pharmacol. Physiol. 36 (2009) 1149–1156.
[18] A.R.K. Sasikala, A.R. Unnithan, Y.-H. Yun, C.H. Park, C.S. Kim, An implantable smart magnetic nanofiber device for endoscopic hyperthermia treatment and tumor-triggered controlled drug release, Acta Biomater. 31 (2016) 122–133.
[19] S. Aziz, M. Hashim, I. Ismail, S. Tamilselvan, N. Alitheen, M. Swamy, B. Purna Chandra Rao, Synthesis, characterization and in vitro evaluation of manganese ferrite (MnFe2O4) nanoparticles for their biocompatibility with murine breast cancer cells (4T1), Molecules 21 (2016) 312.
[20] S.A. Shah, A. Majeed, K. Rashid, S.-U. Awan, PEG-coated folic acid-modified superparamagnetic MnFe2O4 nanoparticles for hyperthermia therapy and drug delivery, Mater. Chem. Phys. 138 (2013) 703–708.
[21] M.Z. Fahmi, J.-K. Chen, C.-C. Huang, Y.-C. Ling, J.-Y. Chang, Phenylboronic acid-modified magnetic nanoparticles as a platform for carbon dot conjugation and doxorubicin delivery, J. Mater. Chem. B 3 (2015) 5532–5543.
[22] G.I. Taylor, Disintegration of water drops in an electric field, Proc. Roy. Soc. Lond. Math. Phys. Sci. 280 (1964) 383–397.
[23] W.G. Glasser, 6. Prospects for future applications of cellulose acetate, in: Macromolecular Symposia, Wiley Online Library, 2004, pp. 371–394.
[24] S.F. Gomaa, T.M. Madkour, S. Moghannem, I.M. El-Sherbiny, New polylactic acid/cellulose acetate-based antimicrobial interactive single dose nanofibrous wound dressing mats, Int. J. Biol. Macromol. 105 (2017) 1148–1160.
[25] V. Beachley, X. Wen, Effect of electrospinning parameters on the nanofiber diameter and length, Mater. Sci. Eng. C 29 (2009) 663–668.
[26] M. Dzikri, T. Armedya, S. Khairunisa, S. Sakti, Y. Raharjo, W. Purnamasari, N. Nasronudin, M. Fahmi, Design of cellulose acetate-collagen nanofiber and its in vitro assessment as wound dressing candidate, Digest J. Nanomater. Biostruct. 14 (2019) 203–212.
[27] S. Megelski, J.S. Stephens, D.B. Chase, J.F. Rabolt, Micro-and nanostructured surface morphology on electrospun polymer fibers, Macromolecules 35 (2002) 8456–8466.
[28] R.W. Korsmeyer, S.R. Lustig, N.A. Peppas, Solute and penetrant diffusion in swellable polymers. I. Mathematical modeling, J. Polym. Sci., Part B: Polym. Phys. 24 (1986) 395–408.
[29] L.L. Lao, S.S. Venkatraman, N.A. Peppas, Modeling of drug release from biodegradable polymer blends, Eur. J. Pharm. Biopharm. 70 (2008) 796–803.

MnFe2O4 nanoparticles/cellulose acetate composite nanofiber for controllable release of naproxen

ORIGINALITY REPORT

11%	7%	12%	2%
SIMILARITY INDEX	INTERNET SOURCES	PUBLICATIONS	STUDENT PAPERS

PRIMARY SOURCES

1	Mochamad Z. Fahmi, Novia F. Sholihah, Aswandi Wibrianto, Satya C.W. Sakti, Fakhri Firdaus, Jia-yaw Chang. "Simple and fast design of folic acid-based carbon dots as theranostic agent and its drug release aspect", Materials Chemistry and Physics, 2021 Publication	2%
2	Tri Prasetyo Armedya, Muhammad Fathan Dzikri, Satya Candra Wibawa Sakti, Abdulloh Abdulloh et al. "Kinetical Release Study of Copper Ferrite Nanoparticle Incorporated on PCL/Collagen Nanofiber for Naproxen Delivery", BioNanoScience, 2019 Publication	2%
3	Zhang, Xiaoli, Keyong Tang, and Xuejing Zheng. "Electrospinning and Crosslinking of COL/PVA Nanofiber-microsphere Containing Salicylic Acid for Drug Delivery", Journal of Bionic Engineering, 2016. Publication	1%

4	pubs.rsc.org Internet Source	1 %
5	cdmf.org.br Internet Source	1 %
6	res.mdpi.com Internet Source	1 %
7	www.ssdsl.gatech.edu Internet Source	1 %
8	www.omicsonline.org Internet Source	1 %
9	Arunima Reghunadhan, Merin S. Thomas, Prasanth K.S. Pillai, Sabu Thomas, Laly A. Pothen. "Bioplastics Used for Nanotechnology Applications", Elsevier BV, 2021 Publication	1 %
10	Salma F. Gomaa, Tarek M. Madkour, Saad Moghannem, Ibrahim M. El-Sherbiny. "New polylactic acid/ cellulose acetate-based antimicrobial interactive single dose nanofibrous wound dressing mats", International Journal of Biological Macromolecules, 2017 Publication	1 %
11	mafiadoc.com Internet Source	1 %

Exclude quotes	On	Exclude matches	< 1%
Exclude bibliography	On		

MnFe2O4 nanoparticles/cellulose acetate composite nanofiber for controllable release of naproxen

GRADEMARK REPORT

FINAL GRADE

/0

GENERAL COMMENTS

Instructor

PAGE 1

PAGE 2

PAGE 3

PAGE 4

PAGE 5

PAGE 6

PAGE 7

PAGE 8